Proceedings of Meetings on Acoustics

Volume 12, 2011 http://acousticalsociety.org/

161st Meeting
Acoustical Society of America
Seattle, Washington
23 - 27 May 2011
Session 2aUWb: Underwater Acoustics

2aUWb11. Mitigation of low-frequency underwater sound using large encapsulated bubbles and freely-rising bubble clouds

Kevin M. Lee*, Kevin T. Hinojosa, Mark S. Wochner, Theodore F. Argo IV and Preston S. Wilson

***Corresponding author's address: Applied Research Laboratories, The University of Texas at Austin, P.O. Box 8029, Austin, TX 78713-8029, klee@arlut.utexas.edu**

Low-frequency anthropogenic noise may affect marine life, motivating the need to minimize its potential impact. Bubbles cause significant dispersion and attenuation of underwater sound at frequencies near the individual bubble resonance and can potentially be used to abate this noise. Such effects have been reported for large encapsulated bubbles with resonance frequencies below 100 Hz, and significant attenuation due to bubble resonance phenomena and acoustic impedance mismatch was observed in a tank experiment [J. Acoust. Soc. Am. 127:2015 (2010); J. Acoust. Soc. Am. 128:2279 (2010)]. Both of these mechanisms were found to significantly reduce down-range radiated acoustic pressure, as much as 40 dB, at low frequencies (60 to 1000 Hz) in a series of lake experiments where a sound source was surrounded by an array of tethered resonant toroidal air bubbles, a cloud of freely-rising sub-resonant bubbles, and various combinations of the two. Hydrophones were placed at various depths and ranges to determine the effect of the bubbles on the radiated field. The effects of void fraction and bubble size variation on the spectrum of the radiated sound were also investigated. [Work supported by Shell.]

Published by the Acoustical Society of America through the American Institute of Physics

 [DOI: 10.1121/1.4711784]
Received 30 Mar 2012; published 20 Apr 2012

1 Introduction

Underwater low-frequency anthropogenic noise from marine vessels and machinery is known to produce noise in the 10 Hz to 1000 Hz frequency range with much of the peak levels occurring below 500 Hz [1]. Examples of noise sources can include underwater pile driving, commercial shipping traffic, construction and potentially operational noise from offshore wind farm installations, and radiated noise from mobile drilling platforms [2,3]. Studies have shown that underwater sound in this frequency range has the potential to affect marine life, with examples including possible changes to marine mammal migratory patterns and interference with inter-animal communication, predation, or other behavioral aspects [4, 5]. Thus, there is a desire to minimize the operational noise footprint of these activities.

A proposed strategy for mitigating anthropogenic underwater noise is to make use of the acoustic properties of air bubbles in water. Two possible mechanisms for attenuation of underwater sound using air bubbles have been investigated: bubble acoustic resonance phenomena and acoustic impedance mismatching between bubbly water and bubble-free water. The first of these mechanisms was studied for large encapsulated gas bubbles using a laboratory waveguide experiment and finite-element modeling [6]. Commander and Prosperetti's effective medium model of sound propagation in bubbly liquids was shown to work well for describing propagation in water containing large stationary encapsulated air bubbles with thin-walled elastic shells [6,7]. Subsequently, quantitative measurements of attenuation of standing waves at low frequencies were performed in a large tank experiment [8]. In these experiments, an underwater sound source was surrounded with various bubble configurations, including both screens or arrays of large tethered stationary encapsulated bubbles and clouds of freely-rising bubbles, and a significant reduction in level of the tank's acoustic response was observed. Additionally, the effect of the thickness of the encapsulating material around the bubbles was also investigated, and it was found that as the shell thickness increased, the amount of sound reduction decreased.

In the work reported here, a series of lake experiments were performed in which large tethered encapsulated bubble arrays and bubble clouds were alternatively employed to determine their efficacy in reducing radiated low-frequency underwater sound. While the smaller freely-rising bubbles attenuated sound at frequencies closer to 1 kHz, the use of encapsulated bubbles was shown to provide up to 40 dB of sound level reduction at frequencies below 500 Hz.

The paper has the following structure. First, the two primary mechanisms for reducing underwater sound using air bubbles are outlined. The apparatus used for the lake experiments is then described. Next, results are presented where freely-rising bubbles, whose resonance frequencies are above the noise frequency range of interest, are used to surround the sound source. The same experiment was

then repeated using stationary arrays of large tethered encapsulated bubbles to surround the sound source. Here, the bubble resonance was chosen to be in the frequency range of interest, such that the bubble resonance mechanism played a much greater role in reducing the radiated sound levels. Finally, conclusions are presented.

2 Mechanisms of sound attenuation using air bubbles

Attenuation by damping and scattering of sound waves near the bubble resonance frequency in a bubbly liquid are described by Commander and Prosperetti's model, which describes an infinite bubbly liquid's interaction with linear plane acoustic waves [7]. The bubbles are assumed to be spherical with radius a and a bubble size distribution function $f(a)$. The individual bubble resonance frequency is given by:

$$\omega_0^2 = \frac{P_{\mathrm{b,e}}}{\rho_\ell a^2}\left(\mathrm{Re}[\Phi] - \frac{2\sigma}{aP_{\mathrm{b,e}}}\right), \tag{1}$$

where $P_{\mathrm{b,e}}$ is the equilibrium pressure at the bubble's surface, ρ_ℓ is the liquid density, a is the bubble radius, the term Φ is related to the dynamics of the bubble as it expands and contracts, and σ is the surface tension of the liquid. Note that larger bubbles have lower resonance frequencies. A resonance frequency of 60 Hz corresponds to a bubble with a radius of approximately 5 cm.

Another important parameter describing the bubbly liquid is the void fraction:

$$\mathrm{VF} = \frac{V_{\mathrm{gas}}}{V_{\mathrm{mixture}}}, \tag{2}$$

which is the ratio of the volume of gas to the total volume of the bubble-liquid mixture.

The complex sound speed for a pressure wave propagating with angular frequency ω in the bubbly liquid is given by:

$$\frac{1}{c_m^2} = \frac{1}{c_\ell^2} + 4\pi\int_0^\infty \frac{af(a)da}{\omega_0^2 - \omega^2 + 2ib\omega}, \tag{3}$$

where c_ℓ is the bubble-free liquid sound speed. The damping term is b, which includes viscous, thermal, and radiation damping terms. For the large bubble sizes needed to resonate at the desired low frequencies, the radiation damping mechanism is dominant, in which the driven bubbles re-radiate the pressure waves in a phase incoherent manner, enabling destructive interference and partial cancellation of the driving waves. The attenuation is given by the imaginary part of the wavenumber:

$$A = 20\left(\log_{10} e\right)\mathrm{Im}\left[k_m\right], \tag{4}$$

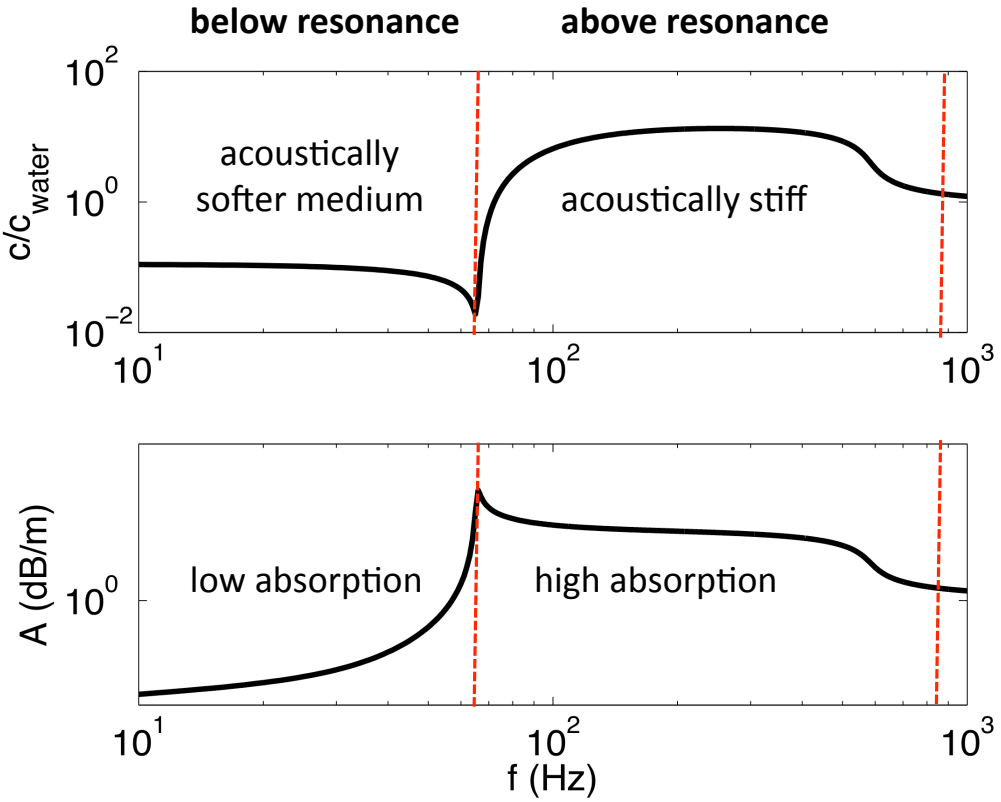

Figure 1: Phase speed and attenuation predicted by the Commander and Propseretti model for a monodisperse distribution of bubbles all with radii of $a = 5$ cm and void fraction VF $= 0.01$.

where the wavenumber is defined as $k_m = \omega/c_m$.

The phase speed and attenuation are plotted in Figure 1 for a monodisperse distribution of 5-cm-radius bubbles. Above the individual bubble resonance frequency, the bubbly liquid is acoustically stiffer than bubble-free water and it offers a high level of attenuation. Below resonance there is low attenuation; however, the medium is acoustically much softer than water, thus there is a large contrast with the acoustic impedance of bubble-free water. This motivates a second sound reduction mechanism that can potentially be exploited below the individual bubble resonance frequency, where the absorption and scattering are relatively weak. A lumped-element electrical circuit analog can be used to explain this impedance contrast mechanism. Suppose the sound source is surrounded by a bubbly liquid, which is itself surrounded by bubble-free water extending out into space. In the circuit analog, the sound source is modeled as a volume velocity source. Two parallel load elements represent the bubble-free water and the bubbles with re-

spective acoustic impedances Z_{water} and Z_{bubble} with $Z_{\text{bubble}} \ll Z_{\text{water}}$. Because more power goes into the low impedance load, less sound if transmitted out into the surrounding water.

3 Experimental apparatus

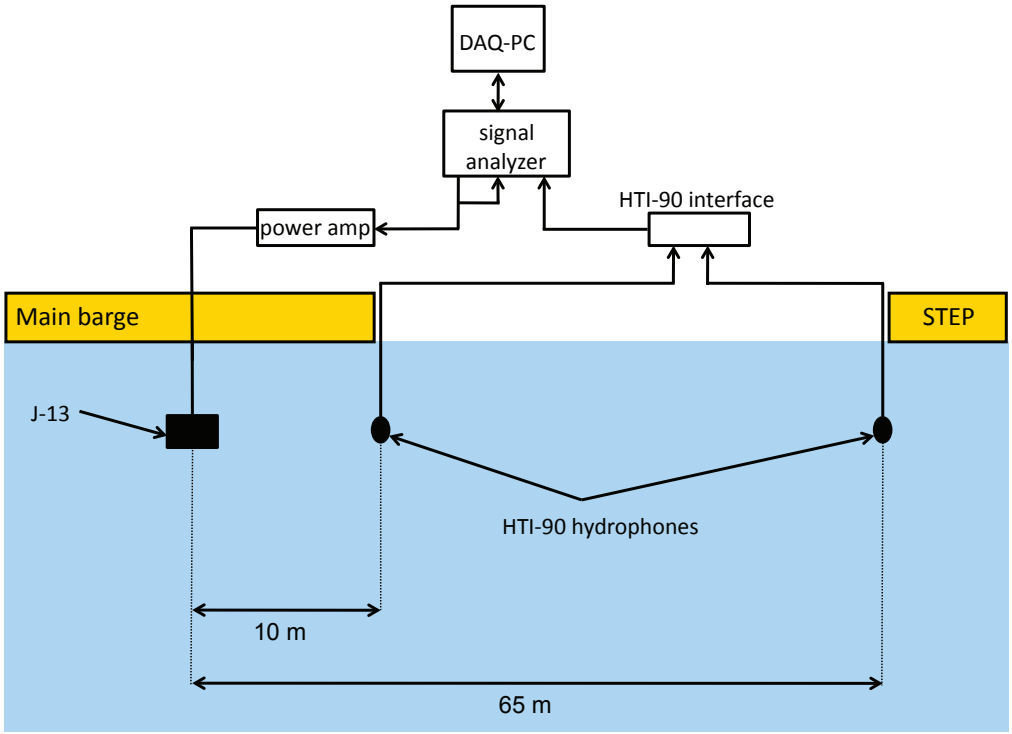

Figure 2: Schematic diagram of the experimental apparatus. The J-13 sound source was suspended from the main barge at a depth of 2.6 m, and the received level at each of the hydrophone locations was determined by measuring the transfer function between the source and each hydrophone. One hydrophone was suspended from the main barge at a horizontal distance of 9.73 m from the sound source, and the other was suspended from the STEP barge at a horizontal distance of 64.5 m. The depth of both receivers could be varied from 2 m to 20 m.

Sound reduction experiments using both freely-rising and large stationary encapsulated bubbles were conducted at the Lake Travis Test Station (LTTS) near the Mansfield Dam in Austin, TX. The basic measurement apparatus is shown in Figure 2. A US-Navy J-13 compact electromechanical acoustic source was suspended from the main barge at LTTS. Two High Tech dual-sensitivity HTI-90-U

hydrophones were used as receivers, with one deployed 9.73 m away from the source of the main barge and one deployed 64.5 m away from the source from a secondary barge named the STEP barge, shown in Fig. 2. The lake depths under the main barge and the STEP barge at the time of the experiments were approximately 25 m and 38 m, respectively. The deployment depth of the sound source for the water surface was 2.6 m. The receiver depths were varied between 2 m and 20 m in 2-m increments.

The source signal was generated by an Agilent 89410-A Vector Signal Analyzer (VSA) and consisted of a continuosly-repeated 800-millisecond-duration periodic chirp ranging in frequency from 60 Hz to 2 kHz, which was sent to a Crown CE4000 power amplifier. In between the J-13 projector and the power amplifier was a custom-built output transformer which matched the electrical impedance between the J-13 input and power amplifier output to maximize the acoustical output of the system. The lower limit of the frequency sweep coincided with the lower limit of the source response. Source current was monitored with a Pearson current transformer to ensure linear operation of the source. The received signal was passed through an analog bandpass filter (20 Hz – 2 kHz) and then to the input of the VSA. The transfer function between source and receiver was computed and averaged over 30 consecutively acquired spectra, and it was then transfered to a computer via a GPIB connection for data storage and later analysis.

4 Freely-rising Bubbles

Freely-rising bubbles were generated using two concentric aeration hose rings that were held by a steel frame approximately 0.5 m below the sound source and approximately 3.5 m below the surface of the water. Continuous air flow was delivered to the aeration hoses by a low-pressure, high flow rate, diesel-powered air compressor. The flow rate for each ring was regulated manually by an adjustable flow meter, which also served the purpose of monitoring the air flow rate. The regulator assembly also included a pressure gauge for each ring to monitor the air pressure as well as valves for shutting off the air flow to each ring. Free bubble generation around the sound source is depicted in Figure 3. The mean bubble radius was estimated to be approximately 0.5 cm or less using underwater photography, and a distribution over of a range of bubble sizes likely exists within the cloud. The void fraction was essentially the only controllable physical parameter for the system. Estimates of the void fraction in the bubble cloud were obtained using the measured air flow rate and the initial rise time of the bubble cloud for a given set of operating parameters. The void fraction was varied between approximately 0.005 and 0.025. The effect of the freely-rising bubbles on the radiated sound is illustrated by comparison of the measured transfer function with and without the

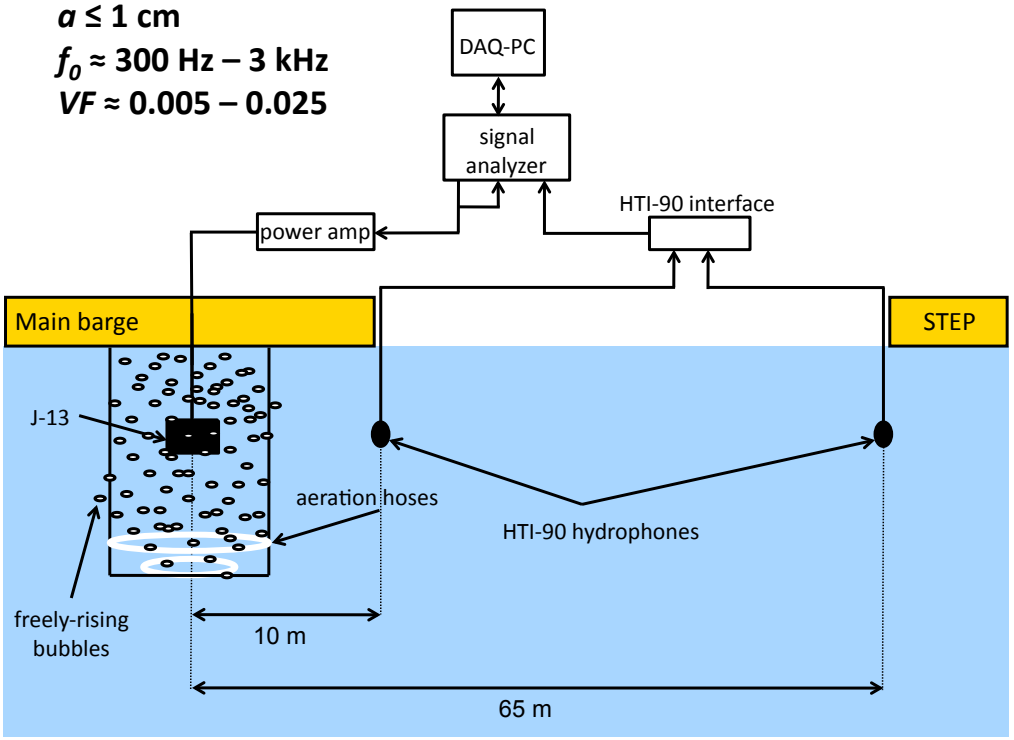

Figure 3: Schematic diagram of the experimental apparatus with freely-rising bubbles enveloping the sound source. Using underwater photography, the bubbles were estimated to have radii of less than 1 cm. The void fraction, which ranged from 0.005 to 0.025, was estimated from the rise time of the bubbles, the compressed air flow rate to the aeration hoses, and the total volume of the region occupied by the bubble cloud.

bubble cloud enclosing the source, as shown in Figure 4. The bubble cloud had a void fraction of approximately 0.02. At the 9.73 m receiver location, a reduction in radiated sound of 4 dB is observed at 60 Hz, and the reduction increases to 23 dB at 100 Hz. Because this is well below the estimated bubble resonance frequency, the reduction here is likely due to primarily the acoustic impedance mismatch between the bubble cloud and bubble-free water. For frequencies between roughly 350 Hz to just over 1 kHz, the received level is reduced to a least the ambient noise level, some 40 dB below the signal level in the bubble-free case. In this frequency band, the attenuation is likely due to a combination of acoustic impedance mismatching and bubble resonance phenomena; however, bubble or cloud resonance effects likely dominate giving rise to the greater noise reduction. At higher frequencies the received level begins to approach the bubble-free case as the resonance mechanism

weakens. The attenuation predicted by the Commander and Prosperetti model is also plotted in Figure 4 for qualitative comparison. The bubble size distribution for the experimental bubble cloud is approximated as being Gaussian with a mean radius of $a_0 = 0.5$ cm and a standard deviation of $\sigma = 0.25a_0$. For the bubble cloud case, the measured attenuation is qualitatively in agreement with the model prediction. Although these results demonstrate that significant sound level reduc-

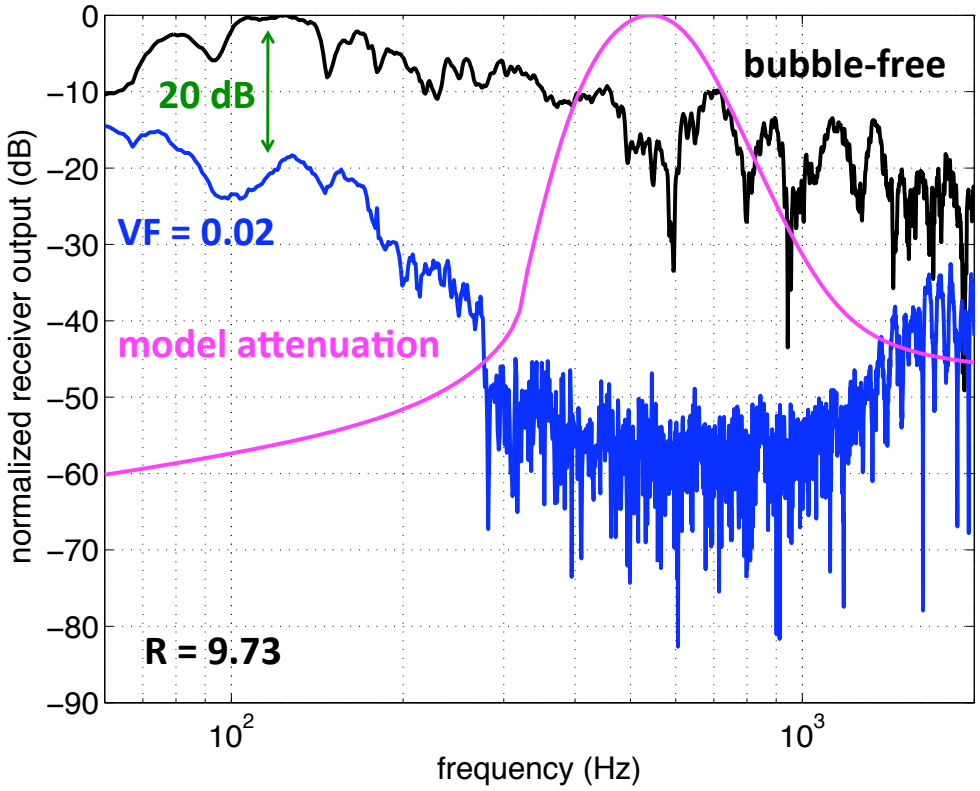

Figure 4: Normalized receiver output with (*blue*) and without (*black*) freely-rising bubbles enveloping the sound source for the hydrophone at located at a horizontal range of 9.73 m. The hydrophones were located at a depth of 10 m. The attenuation predicted by the Commander and Prosperetti (*pink*) model is overlaid for qualitative comparison only with the data. The units for the model prediction do not correspond to the vertical axis values in this figure. The input parameters chosen to approximate the bubble cloud parameters in this case were a Gaussian bubble size distribution with mean radius $a_0 = 0.5$ cm, standard deviation $\sigma = 0.25a_0$, and a void fraction of 0.02.

tion is possible with freely-rising bubbles, the frequencies most greatly affected are often higher than the frequency range of much anthropogenic noise.

5 Stationary encapsulated bubbles

For frequencies below 500 Hz, which coincides with frequencies of many of the industrial noise sources of interest, bubbles that resonate near 100 Hz or below are required, corresponding to those with radii of several centimeters. Unfortunately, free bubbles with spherical geometry, or even spheroidal geometries, are unstable for bubble radii less than 1 cm [9]. Free bubbles with large volumes and non-spheroidal geometries could potentially be used, but these are also known to be unstable and to break up into smaller bubbles [10, 11], thus they are difficult to generate reliably. Additionally, such bubbles, if created, would likely be disrupted or carried away by tides, waves, or ocean currents if deployed in a real-world application in a marine environment.

To address these difficulties, encapsulated bubbles were used. The bubble is created by encapsulating a predetermined volume of air within a thin elastic shell made of some material such as latex. Encapsulated bubbles have several advantages over freely rising bubbles. Because the volume of the bubble is deterministic, the resonance frequency can be chosen with a high degree of accuracy, and the resonance frequency can be made as low as needed. Additionally, they may be tethered and used to form a stationary array or curtain in a predetermined position around the noise source. Thus, screens using encapsulated bubbles are highly designable. The two main requirements of the material used to encapsulate the bubbles are that it must be elastic and thin enough to allow for resonant motion of the encapsulated air volume, and it also needs to be robust enough for deployment in the marine environment.

A schematic of the experiment used to test the effect of encapsulated bubbles on the level of radiated sound is shown in Fig 5. The apparatus is similar to that used with the freely-rising bubbles. The apparatus consisted of a frame constructed of steel struts with sides made of netting to which various configurations of thin-shelled encapsulated bubbles were attached. Two additional panels of netting with encapsulated bubbles attached were included in the interior of the frame. The source was located in the center of the frame at a depth of 2.6 m. The encapsulated bubbles were used to partially fill the volume of water outlined by the frame. The void fraction was defined by the number of encapsulated bubbles N, the mean single bubble volume V_{bub}, and the total volume inside of the frame V_{tot}, $VF = NV_{\text{bub}}/V_{\text{tot}}$. The transfer functions for a bubble-free experimental configuration and three encapsulated bubble configurations are shown in Figure 6. For all three bubble cases the mean bubble radius was $a_0 = 7.2$ cm. The number of encapsulated bubbles tethered to the frame was varied from $N = 35$ to $N = 70$ to $N = 150$ which resulted in void fractions of approximately 0.005, 0.01, and 0.02, respectively. Note that as the number of bubbles or void fraction increases, the received signal level is successively reduced from the bubble-free case by greater

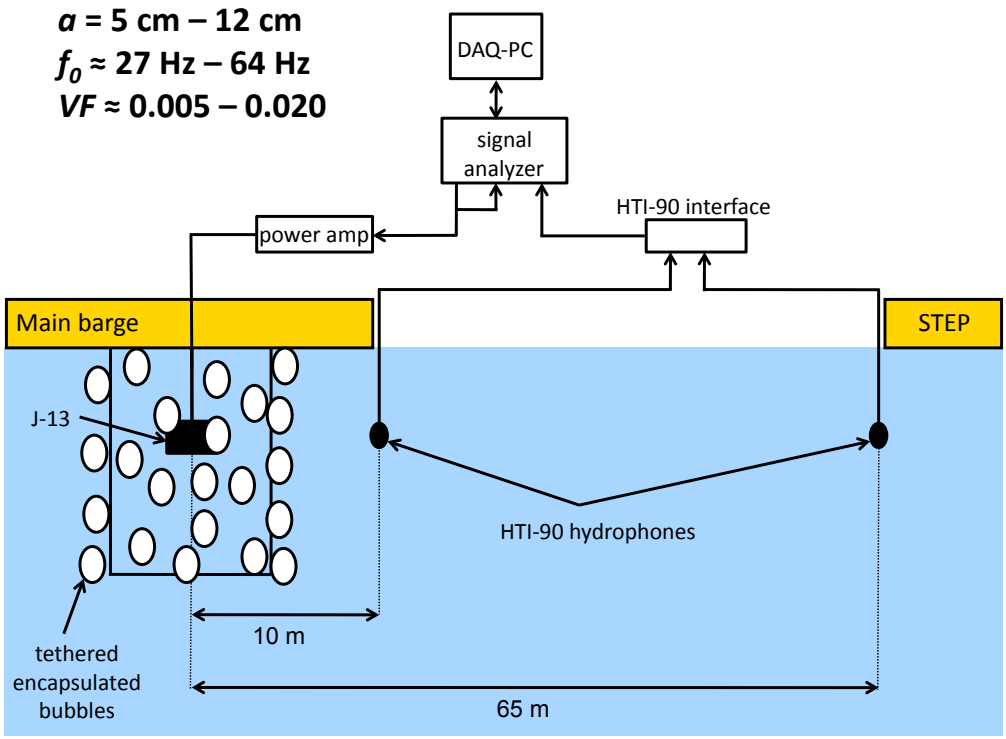

Figure 5: Schematic diagram of the experimental apparatus with tethered encapsulated bubbles surrounding the sound source. The bubble radii used ranged from approximately 5 cm to 12 cm. The void fraction was independently varied from 0.005 to 0.02, by tethering different numbers of encapsulated bubbles around the sound source.

amounts over the entire 60 Hz to 2 kHz frequency range. The peak attenuation is achieved for a void fraction of 2%, where the signal level is reduced by greater than 40 dB at a frequency of approximately 100 Hz. The minimum amplitude for each configuration occurs at nearly the same frequency. Since the bubbles in these configurations had nearly identical radii, the frequencies at which the minima occur are interpreted to correspond to the encapsulated bubble resonance frequencies. For the 7.2-cm-radius bubbles, the resonance frequency is approximately 100 Hz. Control of the frequency band of attenuation is demonstrated in Figure 7. Here, the void fraction for each encapsulated bubble case was held fixed, but the bubble radius was varied from $a_0 = 5.1$ cm to $a_0 = 11.6$ cm. To achieve a void fraction of 0.5%, this required $N = 87$ of the $a_0 = 5.1$ cm bubbles, $N = 35$ of the $a_0 = 7.2$ cm bubbles, and just $N = 10$ of the $a_0 = 11.6$ cm bubbles, each configured separately. The transfer function for the bubble-free case is displayed for reference.

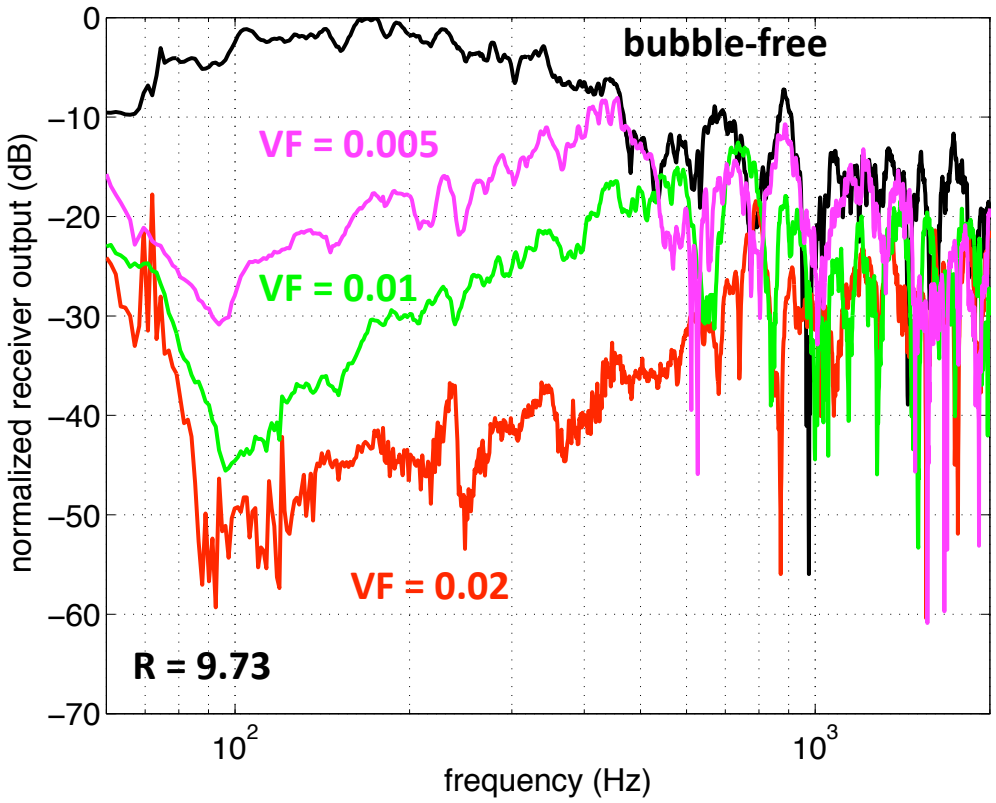

Figure 6: Normalized receiver output with no bubbles (*black*), 35 encapsulated bubbles (*pink*), 70 encapsulated bubbles (*green*), and 150 encapsulated bubbles (*red*) enveloping the sound source. The hydrophones were located at a depth of 10 m and a range of 9.73 m. For all cases the mean bubble radius was 7.2 cm.

As encapsulated bubble size is increased, the range of high attenuation shifts to lower frequencies. Observation of the behavior for the 11.6-cm-radius bubbles was extended below the 60 Hz periodic chirp cutoff using single frequency sinusoidal tones ranging from 30 Hz to 100 Hz in 10-Hz increments. This data was collected to resolve the frequency at which the minimum occurred for the largest-sized bubble case. These data points, along with the transfer functions from Figure 7, are reproduced in Figure 8. For each bubble size the frequency of the minimum amplitude was found for data collected on all of the vertical receiver positions, and an average value was computed. These frequency minimum values are 50.0 Hz, 99.8 Hz, and 170.6 Hz for the 11.6-cm-radius, 7.2-cm-radius, and 5.1-cm-radius encapsulated bubble cases. The bubble resonance frequencies predicted by Eq. (1) for free bubbles with corresponding radii are 28 Hz, 44 Hz, and 63 Hz, respectively. If the observed frequency minima are interpreted as being estimates of the

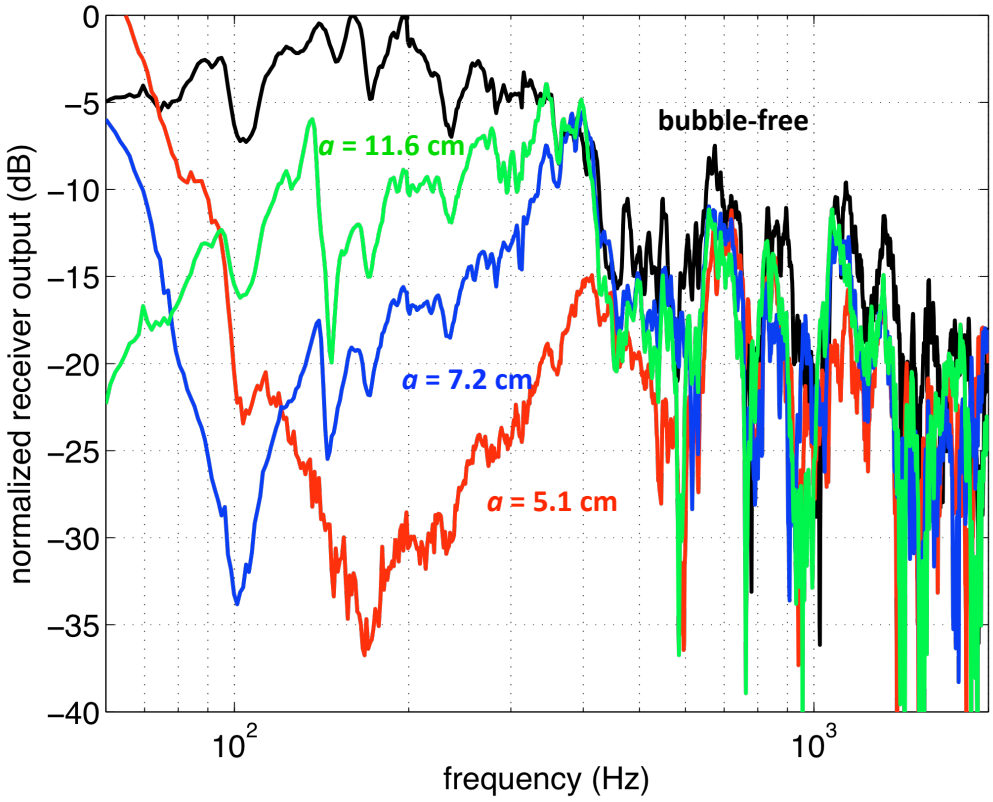

Figure 7: Normalized receiver output with no bubbles (*black*), 87 encapsulated bubbles with $a_0 = 5.1$ cm (*red*), 35 encapsulated bubbles with $a_0 = 7.2$ cm (*blue*), and 10 encapsulated bubbles with $a_0 = 11.6$ cm (*green*) enveloping the sound source. The hydrophones were located at a depth of 12 m and a range of 9.73 m. For all cases the void fraction was 0.005.

encapsulated bubble resonance frequencies, Eq. (1) under-predicts these values by as much as 37.1%. The bubbles in the Commander and Prosperetti model do not have finite-thickness elastic shells, and it is the presence of the shells on the encapsulated bubbles that modify the bubble resonance frequencies from their predicted values.

6 Conclusions

Using a cloud or curtain of freely-rising bubbles as an underwater noise mitigation strategy was shown to achieve as much as 10 to 20 dB of sound reduction below several hundred hertz. The primary mechanism of attenuation in this frequency

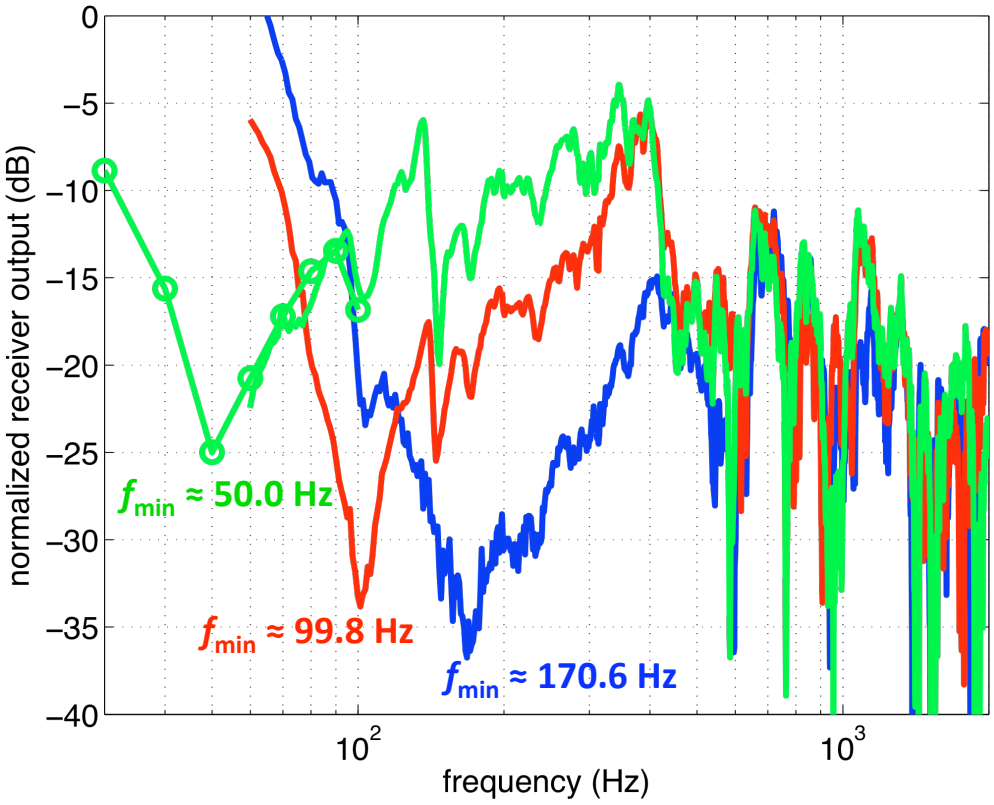

Figure 8: Normalized receiver output with 87 encapsulated bubbles with $a_0 = 5.1$ cm (*red*), 35 encapsulated bubbles with $a_0 = 7.2$ cm (*blue*), and 10 encapsulated bubbles with $a_0 = 11.6$ cm (*green*) enveloping the sound source. The hydrophones were located at a depth of 12 m and a range of 9.73 m. The green curve was extended below 60 Hz with single frequency sinusoidal tones in 10-Hz intervals. For all cases the void fraction was 0.005. The frequency minima for each case are labeled in the figure, and they are interpreted to correspond to the encapsulated bubble resonance frequencies for each bubble size.

range is due to an acoustic impedance mismatch between bubble-free and bubbly water. At higher frequencies closer to the individual bubble resonance frequency, the level reduction was shown to be as much as 40 dB. One drawback to this method is the lack of control over the bubble parameters. The only control parameter was the void fraction, which was altered by changing the airflow rate to the aeration hoses.

Large stationary encapsulated bubbles provide a more effective and targeted approach. More than 40 dB of sound level reduction was observed at frequencies below 200 Hz for the highest void fraction encapsulated bubble configuration.

The degree of control over the system is also greater than that with freely-rising bubbles. The overall sound reduction levels can be controlled simply by adjusting the number of encapsulated bubbles in the array surrounding the sound source. Additionally, different noise frequencies can be targeted by choosing appropriately-sized bubbles to resonate at given frequencies. Furthermore, another degree of control is potentially achievable if combinations of different encapsulated bubble sizes are used to enhance attenuation over a greater number of frequency bands. Additionally, freely-rising bubbles could also be potentially used to enhance the atteunation at higher frequencies closer to 1 kHz.

Overall, the encapsulated bubble strategy can provide a mitigation system that is fully customizable. The system would also be less expensive to implement than using freely-rising bubble sheaths or curtains due to the fact that a continuous air supply is not needed with encapsulated bubbles. Because noise generated from many industrial activities has significant frequency components of a few hundred hertz or below, the larger encapsulated bubbles provide the most targeted noise mitigation solution. [Work supported by Shell Global Solutions.]

References

[1] J. A. Hildebrand, "Anthropogenic and natural sources of ambient noise in the ocean", Mar. Ecol. Prog. Ser. **395**, 5–20 (2009).

[2] N. R. Chapman and A. Price, "Low frequency deep ocean ambient noise trend in the northwest pacific ocean", J. Acoust. Soc. Am. **129**, EL161–EL165 (2011).

[3] C. R. Greene, "Characteristics of oil industry dredge and drilling sounds in the beaufort sea", J. Acoust. Soc. Am. **82**, 1315–1324 (1987).

[4] W. J. Richardson, C. R. Greene, C. I. Malme, and D. H. Thompson, *Marine Mammals and Noise*, 241–322 (Academic Press) (1998).

[5] P. T. Madsen, W. Wahlberg, J. Jougaard, K. Lucke, and P. Tyack, "Wind turbine underwater noise and marine mammals: implications of current knowledge and data needs", Mar. Ecol. Prog. Ser. **309**, 279–295 (2006).

[6] K. M. Lee, K. T. Hinojosa, M. S. Wochner, T. F. Argo IV, P. S. Wilson, and R. S. Mercier, "Sound propagation in water containing large tethered spherical encapsulated gas bubble with resonance frequencies in the 50 Hz to 100 Hz range", J. Acoust. Soc. Am. **130**, 3325–3332 (2011).

[7] K. W. Commander and A. Prosperetti, "Linear pressure waves in bubbly liquids: Comparison between theory and experiments", J. Acoust. Soc. Am. **85**, 732–746 (1989).

[8] K. M. Lee, K. T. Hinojosa, M. S. Wochner, T. F. Argo IV, P. S. Wilson, and R. S. Mercier, "Attenuation of low-frequency underwater sound using bubble resonance phenomena and acoustic impedance mismatching (A)", J. Acoust. Soc. Am. **128**, 2279 (2010).

[9] R. M. Davies and G. I. Taylor, "The mechanics of large bubbles rising through extended liquids and through liquids in tubes", Proc. R. Soc. Lond. A **155**, 375–390 (1950).

[10] G. K. Batchelor, "The stability of a large gas bubble rising through liquid", J. Fluid Mech. **187**, 399–422 (1987).

[11] Y. Fukumoto and Y. Hattori, "Curvature instability of a vortex ring", J. Fluid Mech. **526**, 77–115 (2005).